Supplementary information

Photo-assisted water splitting with bipolar membrane induced pH gradients for practical solar fuel devices

David A. Vermaas, Mark Sassenburg, Wilson A. Smith

Theoretical potentials in bipolar membrane water splitting

As a bipolar membrane allows to face electrolytes with a different pH at either side, an electrical potential difference is established over the bipolar membrane. Assuming an perfectly selective membrane, this potential difference ($\Delta\phi_{BPM}$, in V) equals 0.059 times the pH difference over the membrane, plus the ohmic loss:

$$\Delta\Phi_{BPM} = 0.059 \cdot \Delta pH + i \cdot R \quad (1)$$

In which $\Delta pH = pH_{anode} - pH_{cathode}$, i is the current density (A/cm^2) and R is the area resistance of the membrane ($\Omega \cdot cm^2$).

The voltage over the membrane, due to the pH difference between anode and cathode, causes an equal shift in redox potential for the hydrogen and oxygen evolution reaction:

$$\Phi_{O_2} = 1.23 - 0.059 \cdot pH_{anode} \quad (2)$$

$$\Phi_{H_2} = 0 - 0.059 \cdot pH_{cathode} \quad (3)$$

In which Φ is the potential for oxygen or hydrogen evolution disregarding photovoltage or overpotentials (V). The total bias over the cell is given by $\Phi_{total} = \Phi_{O2} + \Delta\Phi_{BPM} - \Phi_{H2}$. Substitution of eq. 1, 2, 3 and ΔpH yields a total voltage bias of $1.23 + i \cdot R$, as the voltage over the membrane due to the pH difference cancels the pH dependent terms in eq. 2 and 3. In other words, the total bias over the cell, assuming an ideal membrane, is not increased nor decreased by the water dissociation in the bipolar membrane.

Experimental details

Electrochemical measurements

To analyse the solar driven bipolar membrane cell, cyclic voltammetry, linear scan voltammetry and chronoamperometry were applied, controlling the potential between the $BiVO_4$ sample and the corresponding reference electrode (PARstat MC, Princeton Applied Research). Simultaneously, the voltage between the two reference electrodes (i.e., over the bipolar membrane) and the voltage between the anode and cathode were measured. Hence, these synchronized measurements allowed us to calculate the potential of the cathode versus the corresponding reference electrode as well. An illustration of the measured potentials is provided in Fig. S1. Three voltages were measured

simultaneously in the bipolar membrane solar fuel cell, indicated by V_1, V_2 and V_3 in Fig. S1. The fourth voltage, V_4, was calculated using the measured potentials in the following way. The potential of the reference electrode in the cathodic compartment (at pH 0) was defined as zero with respect to the standard hydrogen electrode (SHE). This conversion was done according to:

$$\Phi_{SHE} = \Phi_{Ag/AgCl} + 0.197 \quad (4)$$

In which $\Phi_{Ag/AgCl}$ is the potential of the Ag/AgCl reference electrode (V).

The voltage over the bipolar membrane, Φ_{BPM} (V), is measured by the difference between the reference electrodes at either sides of the membrane. For the potential of the anode, Φ_{anode} (V), the voltage between the anode and the reference electrode in the anodic compartment is added to ϕ_{BPM}. Also the voltage over all component (i.e., Φ_{anode} - $\Phi_{cathode}$) is measured. As $\Phi_{cathode}$ is already known, $\Phi_{cathode}$ can be determined as well.

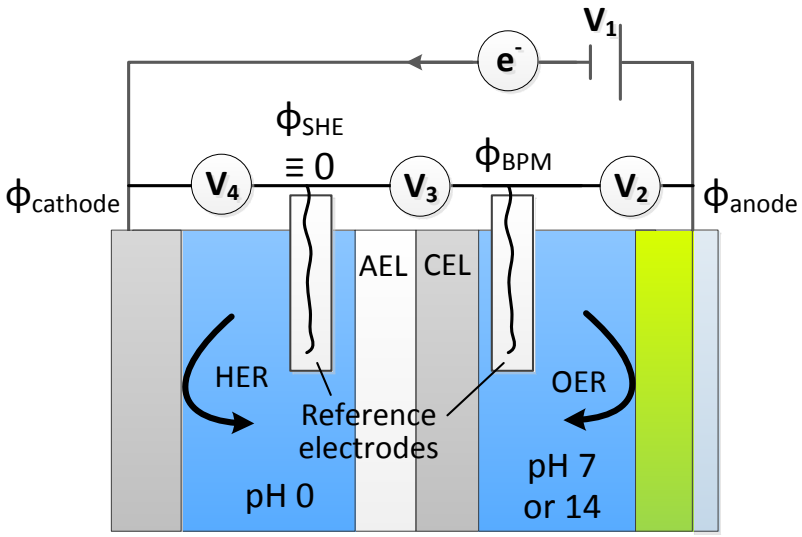

Figure S1: Voltage measurements in bipolar membrane solar fuel cell.

Cyclic voltammetry was performed in dark and illuminated conditions at 50 mV/s for three cycles, where only the third cycle is shown here. During linear scan voltammetry (at 10 mV/s), the illumination source was chopped (5s on, 5s off). To obtain the voltages V_2, V_3 and V_4 in a single graph (i.e., Fig. 2 and 3), potentials are obtained from three synchronized potentiostats as illustrated in Fig. S1, during linear scan voltammetry over the anode at 10 mV/s, using the averaged final 1.5 s of each 5s illumination period. Only current densities > 0.3 mA/cm^2 are considered, to ensure that temporal oxygen concentrations near the Pt cathode do not influence the voltages.

During chronoamperometry, the sample was always illuminated. To evaluate the bipolar membrane, additional measurements using chronopotentiometry were performed. The current density was set for at least 450 s for each current density, in order to stabilize the potential over the membrane.

Voltammetry of $BiVO_4$ samples

Fig. S2 shows the current density of $BiVO_4$ photoanodes at pH 7 and pH 14 under illumination, derived from cyclic voltammetry (Fig. S2A) and chopped-illuminated linear scan voltammetry (Fig. S2B). Fig. S2A shows an onset potential of approximately 0.55 V at pH 7, and the current density in the anodic scan increases to 2.7 mA/cm^2 at 1.23 V, which is similar to previous research for undoped $BiVO_4$ photoanodes with a Co-Pi co-catalyst [1-4]. The cathodic scan shows a significantly lower current density than the anodic scan, in particular between 0.7 and 1.3 V vs RHE. At these same potentials, the linear scan voltammetry with chopped illuminations shows a decreasing transient for each illuminated period (Fig. S2B). Both features are explained by recombination of accumulated holes in the $BiVO_4$ bulk, at the $BiVO_4$ surface [2] or recombination via oxidation products [5].

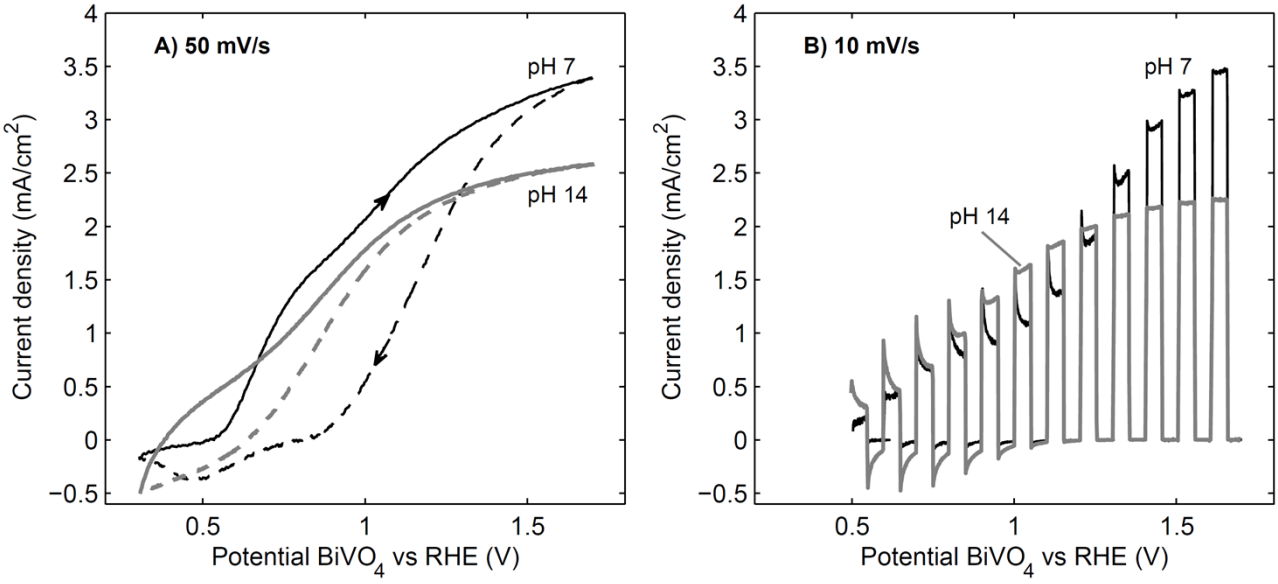

Figure S2: current density vs potential curves for $BiVO_4$ photoanodes operating in pH 7 and pH 14, from illuminated cyclic voltammetry at a scan rate of 50 mV/s (A) and chopped illuminated linear scan voltammetry at 10 mV/s (B). The sample at pH 7 was decorated with Co-Pi, while the sample at pH 14 was covered with TiO_2 and Co-Pi. The cathode, at the other side of the bipolar membrane, operates at pH 0 in both cases. The shown cyclic voltammetry curves are obtained during the 3rd scan, in which the solid line is the anodic scan and the dashed line the cathodic scan.

At pH 14, an anodic current is already observed at a potential of 0.35 V vs RHE, but is likely due to a redox wave of the TiO_2, caused by the redox reaction between Ti^{4+} and Ti^{3+} in the defect-rich TiO_2 [6]. This hypothesis is consistent with the linear scan voltammetry with chopped illumination (Fig. S2B), where a transient cathodic current is observed during dark segments. This effect disappears at higher potentials, where Ti^{4+} is no longer reduced to Ti^{3+}, and the anodic current can be ascribed to water oxidation.

Apart from the high current density at potentials below 0.7 V, the anodic scan shows a slightly lower current density than at pH 7 (Fig. S2A). The lower current density for the anodic scan is possible due to the transformation of the Co-Pi co-catalyst at high pH to cobalt oxide (CoO_x) [7] even though cobalt oxide still has good catalytic activity for oxygen evolution [8]. Other catalysts, such as nickel (iron)

hydroxides, may yield higher current densities in strongly alkaline media [8, 9], but are not applied in this research to minimize the differences between the shown samples.

The $BiVO_4$ photoanode is reasonably stable in pH 7 for at least 1 hour, while the observed current density is unstable in pH 14 (Fig. S3). The initial decrease in current density for pH 7 is due to the hole accumulation and recombination as described in Fig. S2, and the current density stabilizes for the remaining 50 minutes. At pH 14, however, the TiO_2 protection layer cannot prevent photocorrosion of $BiVO_4$. Previous research of $BiVO_4/TiO_2$ reported a stable photocurrent at pH 10.4 and sample-to-sample variable results (due to pinhole defects) at pH 13 [10]. Pinhole defects in the TiO_2 layer are even more critical in this research using such alkaline solution (1 M KOH).

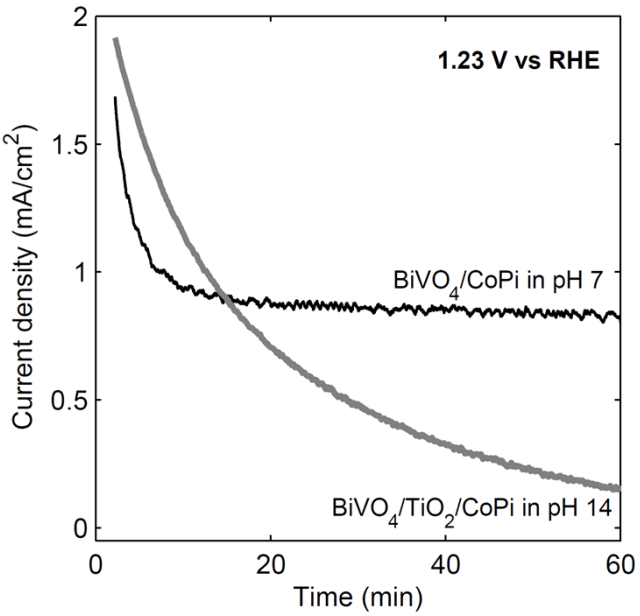

Figure S3: Current density against time, derived from chronoamperometry at 1.23 V vs RHE and illuminating with 100 mW/cm², for $BiVO_4$ with CoPi in pH 7 and $BiVO_4$ with TiO_2 and CoPi in pH 14.

As a bias was applied to facilitate the water splitting, no solar-to-hydrogen (STH) efficiency can be derived from this exact system. However, when envisioning a bias-free system using a photovoltaic (PV) cell behind a $BiVO_4$ photoanode, as demonstrated before [1], and 100% Faradaic efficiency, the STH efficiency can be estimated. The intersections of the i-v curves for a 2-jn a-Si PV cell and that for the $BiVO_4$ photoanodes as shown in Fig. S4 provide such an estimate for the STH efficiency. This STH efficiency is similar or slightly higher for the BPM-cell compared to when using no membrane at all.

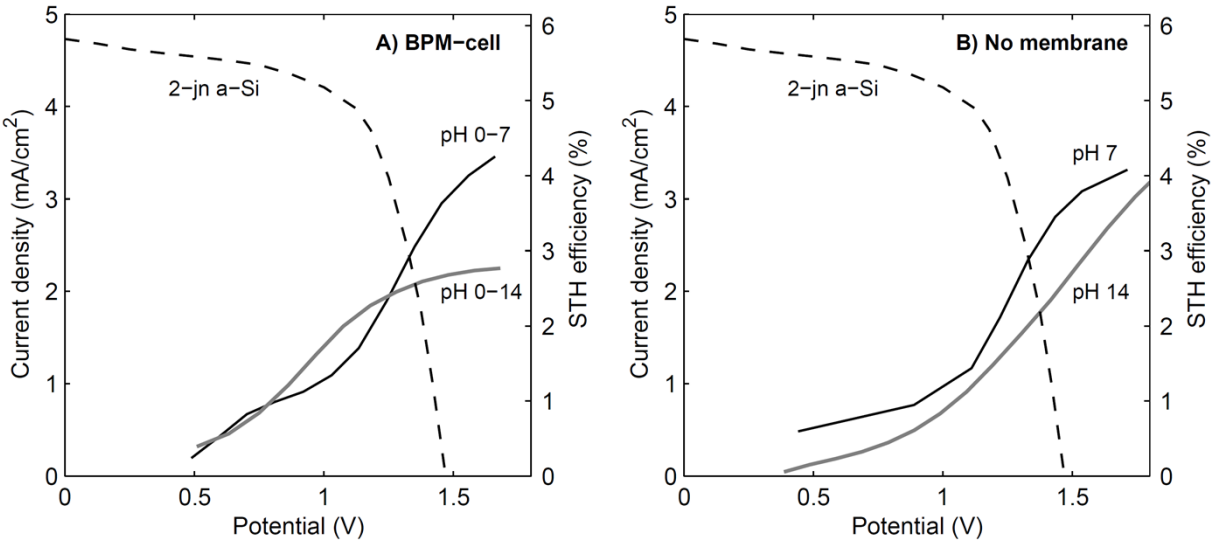

Figure S4: Current density as a function of voltage over a BPM-cell (A) or a membrane-less system (B), using Pt cathode and a $BiVO_4$/CoPi anode (pH 7) or $BiVO_4/TiO_2$/CoPi anode (pH 14). When using a BPM (graph A), the Pt cathode operates in pH 0. The dashed graphs indicate the i-v curve of a 2-jn a-Si photovoltaic (PV) cell, as derived from previous research to a $BiVO_4$-PV tandem [1]. The intersections between the solid and dashed lines indicate the estimated STH efficiency of the present system.

Oxygen evolution

Oxygen evolution was measured using gas chromatography (Interscience Trace 1300/1310 series) while purging the anodic electrolyte with N_2 gas (99.999% pure) at 7.8 sccm and holding a $BiVO_4$/CoPi sample in pH 7 electrolyte at 1.23 V vs RHE for 60 minutes. The measured oxygen concentrations in the effluent gas are measured and converted to current density. This current density, derived from the O_2 production, is compared to the measured current density from the potentiostat in Fig. S5.

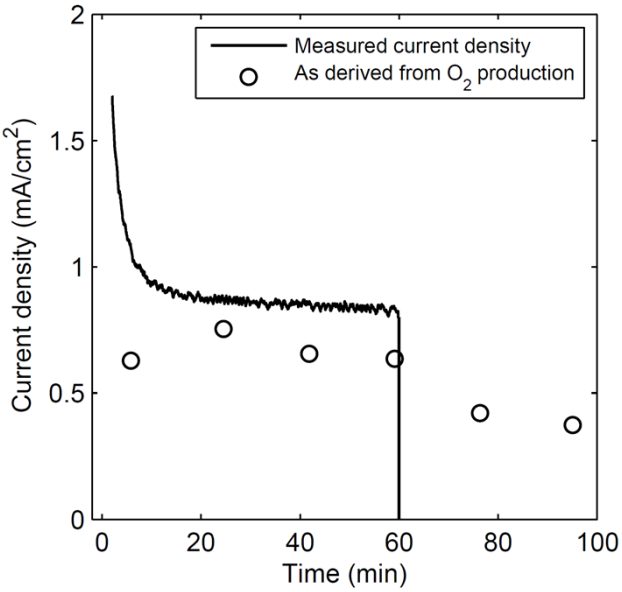

Figure S5: Current density as measured at potentiostat (solid line) and as derived from O_2 measurements (circles), for $BiVO_4$/CoPi at pH 7 and 1.23 V vs RHE.

As the water volume in this lab-scale device is large with respect to the sample size, the oxygen evolution is diffused over time. This causes a slightly lower Faradaic efficiency, in particular near the start of the experiment. However, when the current is stopped after 60 minutes, oxygen is still detected in the effluent, indicating that the actual produced oxygen is close to the quantity expected from a 100% Faradaic efficiency.

References

1. F. F. Abdi, L. Han, A. H. M. Smets, M. Zeman, B. Dam and R. van de Krol, *Nat Commun*, 2013, **4**.
2. F. F. Abdi and R. van de Krol, *The Journal of Physical Chemistry C*, 2012, **116**, 9398-9404.
3. S. K. Pilli, T. E. Furtak, L. D. Brown, T. G. Deutsch, J. A. Turner and A. M. Herring, *Energy & Environmental Science*, 2011, **4**, 5028-5034.
4. D. K. Zhong, S. Choi and D. R. Gamelin, *Journal of the American Chemical Society*, 2011, **133**, 18370-18377.
5. D. Eisenberg, H. S. Ahn and A. J. Bard, *Journal of the American Chemical Society*, 2014, **136**, 14011-14014.
6. P. Salvador, M. L. Garcia Gonzalez and F. Munoz, *The Journal of Physical Chemistry*, 1992, **96**, 10349-10353.
7. T. H. Jeon, W. Choi and H. Park, *Physical Chemistry Chemical Physics*, 2011, **13**, 21392-21401.
8. C. C. L. McCrory, S. Jung, J. C. Peters and T. F. Jaramillo, *Journal of the American Chemical Society*, 2013, **135**, 16977-16987.
9. M. J. Kenney, M. Gong, Y. Li, J. Z. Wu, J. Feng, M. Lanza and H. Dai, *Science*, 2013, **342**, 836-840.
10. M. T. McDowell, M. F. Lichterman, J. M. Spurgeon, S. Hu, I. D. Sharp, B. S. Brunschwig and N. S. Lewis, *The Journal of Physical Chemistry C*, 2014, **118**, 19618-19624.